Author(s): Berseneva, Natalia & Krasheninnikov, Arkady V. & Nieminen, Risto M.

Title: Mechanisms of Postsynthesis Doping of Boron Nitride Nanostructures with Carbon from First-Principles Simulations

Year: 2011

Version: Final published version

Please cite the original version:

Berseneva, Natalia & Krasheninnikov, Arkady V. & Nieminen, Risto M. 2011. Mechanisms of Postsynthesis Doping of Boron Nitride Nanostructures with Carbon from First-Principles Simulations. Physical Review Letters. Volume 107, Issue 3. 035501/1-4. ISSN 0031-9007 (printed). DOI: 10.1103/physrevlett.107.035501.

Mechanisms of Postsynthesis Doping of Boron Nitride Nanostructures with Carbon from First-Principles Simulations

Natalia Berseneva,[1] Arkady V. Krasheninnikov,[1,2] and Risto M. Nieminen[1]

[1]*Department of Applied Physics, Post Office Box 1100, FI-00076 Aalto University, Finland*
[2]*Department of Physics, University of Helsinki, Post Office Box 43, FI-00014, Finland*

(Received 24 February 2011; revised manuscript received 2 May 2011; published 11 July 2011)

Electron-beam-mediated postsynthesis doping of boron-nitride nanostructures with carbon atoms [Nature (London) **464**, 571 (2010); J. Am. Chem. Soc. **132**, 13 692 (2010)] was recently demonstrated, thus opening a new way to control the electronic properties of these systems. Using density-functional theory static and dynamic calculations, we show that the substitution process is governed not only by the response of such systems to irradiation, but also by the energetics of the atomic configurations, especially when the system is electrically charged. We suggest using spatially localized electron irradiation for making carbon islands and ribbons embedded into BN sheets. We further study the magnetic and electronic properties of such hybrid nanostructures and show that triangular carbon islands embedded into BN sheets possess magnetic moments, which can be switched on and off by electrically charging the structure.

DOI: 10.1103/PhysRevLett.107.035501 PACS numbers: 61.80.Fe, 61.72.J−, 61.82.Bg, 73.63.−b

Graphene [1] is a two-dimensional (2D) material with a honeycomblike arrangement of carbon atoms. Its unique mechanical and electronic properties [2] have stimulated vigorous research on possible applications of graphene in nanoelectronics. Concurrently with the studies of graphene, individual flakes of hexagonal boron-nitride (*h*-BN) were isolated and characterized [3,4]. This material has the same hexagonal atomic network as graphene, but alternating boron and nitrogen atoms substitute for carbon. This system is a semiconductor with a gap of more than 5 eV [5], while graphene is a semimetal.

Taking into account the similarities in the atomic structure of these two materials and differences in the electronic characteristics, it is tempting to explore the possibilities for creating hybrid BCN nanosystems, with the electronic properties defined by the relative concentration of B, C, and N atoms. Numerous attempts to manufacture graphene with nitrogen or boron dopants have indeed been made [6–8], including chemical vapor deposition growth of BCN sheets [9]. However, it was shown [10] that such hybrid materials are thermodynamically unstable and that *h*-BN and graphene tend to segregate, as also confirmed by theoretical studies [11]. An alternative approach to engineering the composite BCN 2D materials was recently demonstrated [12,13]. Post-synthesis substitutional carbon doping of *h*-BN sheets [13] and BN nanotubes [12] was implemented via *in situ* electron-beam irradiation inside a transmission electron microscope (TEM), with the system being transformed from electrical insulator to conductor. It was found that carbon atoms coming from the decomposition of hydrocarbon molecules take mostly the positions of boron atoms, and it was deemed that the substitution process is dominated by the knock-on electron damage followed by mending of the boron-vacancies with carbon atoms. Such an interpretation, however, is inconsistent with nearly the same probabilities for knocking out B and N atoms [14,15] at high (300 keV) electron energies used in the experiments. Moreover, using essentially the same technique, C impurities were introduced into BN sheets at electron energies of 60 keV [16], which is below the threshold for any atom displacement [14,15].

In this Letter, by employing *ab initio* simulations, we show that although radiation damage should definitely play a role in the substitution process, the main driving force for the substitution is the energetics of the system, as it costs less energy to substitute a B-atom than N, especially when the system is positively charged. Taking into account recent experimental results reporting the development of triangular multivacancies under the beam, we further study the electronic structure of triangular carbon islands in BN sheets, and show that, in perfect agreement with Lieb's theorem [17], such quantum dots possess magnetic moments which can be switched on and off by charging the system.

In our simulations we used the spin-polarized density-functional theory (DFT) as implemented in the plane-wave-basis-set VASP [18] code. We used projector-augmented wave potentials [19] to describe the core electrons and the generalized gradient approximation of Perdew, Burke, and Ernzernhof (PBE) [20] for exchange and correlation. As the PBE approach normally underestimates the band gap width, more accurate calculations were also carried out using the Heyd-Scuseria-Ernzerhof (HSE) functional [21]. A kinetic energy cutoff of 400 eV was used in all simulations. We used supercells of different sizes (32–200 atoms) with different numbers of B and N atoms substituted with C atoms. The **k** points for the integration over the Brillouin zone were generated by the Monkhorst-Pack scheme with the account for the supercell size. Such a simulation setup has been demonstrated to be adequate for

the modeling of defects and impurities in 2D systems with covalent bonding [15,22,23]. The finite-supercell-size corrections [24–26] for charged configurations were analyzed by extrapolating the total-energy results to the dilute limit, converging the formation energies within 0.2 eV. The DFT molecular dynamics (MD) simulations of atom dynamics after electron impacts were carried out as in Ref. [15].

The examples of the studied structures are shown in Fig. 1. Throughout this paper, we use the following notations: C_B means that a single B atom was substituted with C atom, while $4C_{3B1N}$ stands for a triangular island formed by substituting 3 B and 1 N atoms with 4C atoms, *etc*. As expected, the PBE calculations for a pristine *h*-BN sheet underestimate the gap (4.56 eV), while the HSE functional provides a semiconducting gap of 5.56 eV, the value which is in a good agreement with the results of quasiparticle GW calculations [27].

We base our analysis of the electron-beam-mediated substitution process on calculations of the formation energy E_f of substitutional defects composed from K_C carbon atoms embedded into the *h*-BN matrix as follows:

$$E_f(K_C^q) = E_{\text{tot}}(K_C^q) - E_{\text{tot}}(\text{BN}) + K_B\mu_B + K_N\mu_N - K_C\mu_C + q(\mu_e - E_V), \quad (1)$$

where $E_{\text{tot}}(K_C^q)$ and $E_{\text{tot}}(\text{BN})$ are the total energies of an *h*-BN system with defect and defect free structure, respectively; K_B and K_N are the numbers of B and N atoms replaced by K_C C atoms ($K_B + K_N = K_C$). μ_B, μ_N, and μ_C are the chemical potentials of the elements present in the system. In an *h*-BN sheet in equilibrium

$$\mu_{\text{BN}} = \mu_B + \mu_N, \quad (2)$$

where μ_{BN} is the total energy per BN pair in the *h*-BN sheet. We chose μ_C the same as in graphene. The choice of μ_B and μ_N is normally defined by the growth conditions of a material. However, here we deal with post-growth conditions and assume that the original system is stoichiometric. As N_2 molecules should be present in the experiments due to imperfect vacuum conditions (note that C atoms in graphene sheets are sometimes substituted with N atoms in a TEM [8]), we assume an N-rich environment, so that μ_N is the same as in the N_2 molecule. q in Eq. (1) is the charge state of the defect complex, and μ_e is the electron chemical potential defined with the same reference as the valence band maximum E_V.

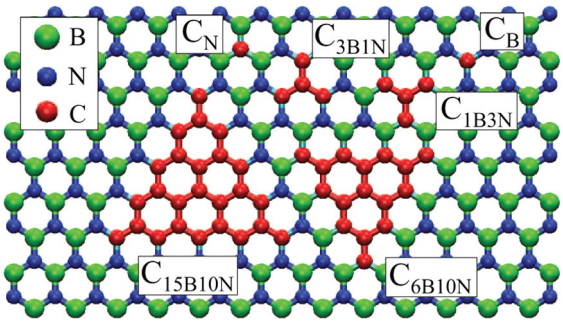

FIG. 1 (color online). Examples of the structures studied in our calculations, including single carbon atom impurities in the *h*-BN sheet, four carbon atom islands with boron ($4C_{1B3N}$ structure) and nitrogen ($4C_{3B1N}$) termination, as well as 16-atom ($16C_{6B10N}$ structure) and 25-atom ($25C_{15B10N}$ structure) islands.

In Figs. 2(a)–2(d) we present formation energies (for the entire system) of four substitutional defects in different charge states as functions of μ_e in the N-rich environment. The results for a single carbon atom in B-atom and N-atom positions agree well with the data for BN nanotubes [28]. It is evident that in the neutral state E_f is always smaller when more B than N atoms are substituted with C. Moreover, for positive charge states, E_f for C_B and $4C_{3B1N}$ goes further down and even becomes negative. This result can be qualitatively understood by taking into account the changes in the total electronic charge of the system: when a B atom is substituted with a C atom, one extra electron is added, and the removal of one electron (charge state "+1") minimizes the local perturbation in the electronic structure caused by the substitution. Note that under high energy electron irradiation an atomically thin target tends to be *positively* charged due to emission of secondary electrons. However, if μ_e is shifted towards the

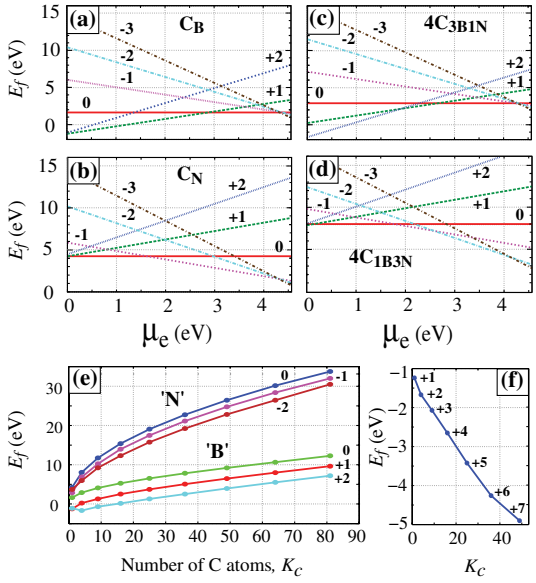

FIG. 2 (color online). Formation energies E_f of substitutional defects in different charge states as functions of electron chemical potential μ_e (a)–(d). Single carbon atom substitutional impurity in B-atom (a) and N-atom (b) positions. Four C atoms substituting 3 B and 1 N-atom (c) and 1 B and 3 N atoms (d). All the results are for the 200-atom supercell with different defects (PBE calculation). The numbers stand for the charge states. E_f as a function of K_C for various charge states and for preferential substitution of N and B atoms (e). E_f vs K_C for positive charge states and for preferential B substitution giving the lowest formation energies for each K_C (f). Note that the values of E_f are negative.

conduction band E_C [e.g., $\mu_e = 3$ eV for preferential N substitution, as in Fig. 2(e)], then substitution of N atoms is also possible indicating that by charging the structure during irradiation, an additional control over substitution process can be gained.

We received qualitatively the same results for all other structures we studied (up to 81 C atoms in the 200-atom BN supercell): it is energetically favorable to have an N-terminated triangular defect with a larger number of missing B atoms, especially for positive charge states of the system, as evident from Figs. 2(e), 2(e), and 2(f) We further studied effects of charging on the energetics of the substitution process by comparing the total energies of neutral and charged reference systems including a C adatom on pristine BN sheet as well as those with C atoms in substitutional positions and the corresponding B/N adatoms on BN sheet. In agreement with the results of E_f calculations presented in Fig. 2, we found that positive charge makes the energy required to "swap" a B atom with a C lower than to swap an N with a C atom, while negative charge gives the opposite result.

Keeping in mind the well-known deficiencies of the DFT-PBE approach, we checked the formation energies of the substitutional defects presented in Fig. 2 by repeating the calculations in a 32-atom supercell using the HSE functional. Figure 3 shows the lowest (among all charge states) formation energies of the substitutional defects presented in Fig. 2 as functions of μ_e calculated using the PBE and HSE functionals. Here the range of μ_e is normalized to the corresponding value of the gap. The PBE and HSE results agree well, indicating that the PBE approach can be used for the calculations of the formation energy of substitutional defects in BN systems if μ_e is rescaled using the ratio of the PBE and HSE gaps.

Although the N-rich environment matches better the experimental situation, we also studied the dependence of the results on the choice of μ_B up to the B-rich environment by the example of substitutional impurities formed by single C atoms. We found that even if $\mu_B = -7.62$ eV corresponding to the lowest energy α-rhombohedral phase of boron [29] is taken as the reference, the substitution of B atoms is still preferable for positively charged systems.

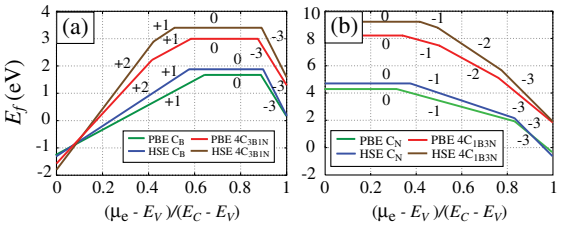

FIG. 3 (color online). Lowest formation energies of the substitutional defects presented in Fig. 2 in different charge states as functions of μ_e calculated using the PBE and HSE functionals. Defects with nitrogen (a) and boron (b) termination. μ_e is normalized to the corresponding value of the gap. It is evident that the PBE and HSE results agree well.

The lower formation energies of defects with N termination are consistent with the preferential substitution of B atoms reported in the experiments [12,13]. Moreover, the energetics may actually explain why mostly B atoms are substituted, as the asymmetry cannot be understood simply as a dynamical effect: at electron energies of 300 keV used in the experiments the cross section for knock out of B and N atom is roughly the same [14,15], so that if C atoms simply take the place of missing atoms at vacancies, the ratio of B/N atoms should be the same as before irradiation. Our results indicate that substitution of B atoms may be thermodynamically preferable, so that irradiation may simply facilitate the substitution process by driving the system away from equilibrium (electrons with impact parameters exceeding the knock-out value transmit kinetic energy to the recoil atoms, which may be high enough for local chemical reactions, e.g., to swap host and C atoms), and may explain the apparent contradiction. The fact that C impurities were introduced into BN sheets at electron energies below the knock-out threshold [16] also indicates that irradiation-mediated reactions can occur, opening new avenues for irradiation-assisted engineering of nanostructures [30].

Nevertheless, to assess the role of kinetics, we calculated the displacement threshold T_d for C impurities and the neighboring B and N atoms. T_d is the minimum kinetic energy transferred to an atom in the system required to sputter the atom. T_d governs the displacement rate, and the corresponding electron threshold energy can be estimated [14,15]. We found that T_d for the C atom is 1.5 eV less than for B atom in the pristine system (independent of the type of the neighboring atoms), giving rise to a 40% increase in the displacement rate (for 300 keV used in the experiments) as compared to that for a B atom in the pristine material. This means that substitution of individual atoms can hardly be explained by dynamical effects only. T_d for the neighboring B atoms (C_N defect) drops by 1.2 eV, and by 3.6 eV for N atoms (C_B defect) as compared to the corresponding values in the pristine system. The displacement rates for these atoms will increase by 20%–30%, which may facilitate the growth of triangular defects. We stress, however, that the actual substitution process may be more complicated, and involve beam-stimulated chemical reactions. Overall, it is much easier to explain the experimental results by the thermodynamics than kinetics of the systems.

Finally, we studied the electronic structure and magnetic properties of substitutional defects representing individual C atoms and triangular islands embedded into the h-BN matrix. The latter may be manufactured if a triangular vacancy-type defect is produced first in a BN sheet by irradiation, [31,32] then carbon deposition, or by focusing the beam in a certain area when hydrocarbon molecules are deliberately introduced into the TEM chamber [12,13]. It was predicted that freestanding triangular graphene flakes of finite sizes should exhibit intriguing magnetic properties [33].

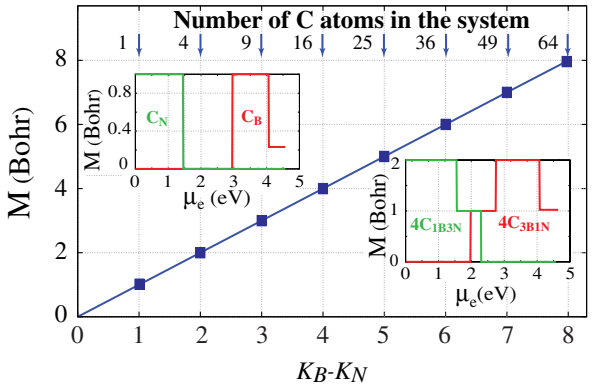

FIG. 4 (color online). Magnetic moments of triangular carbon islands embedded into BN matrix as a function of the difference of the number of substituted nitrogen (K_N) and boron (K_B) atoms. The insets show the magnetic moments of individual C atoms and four-atom defects as a function of μ_e. Green and red lines correspond to preferential N/B substitution. Depending on the defect type, the magnetic moment can be switched on and off.

We found that such structures, if produced, should be stable and that although *h*-BN is a nonmagnetic material, BN sheets with triangular carbon islands possess magnetic moments. The value of the moment depends on the number of substituted atoms and naturally on the charge state of the defect. Figure 4 shows the magnetic moments of the defects as a function of the difference of the number of substituted nitrogen (K_N) and boron (K_B) atoms. The removed B and N atoms can be associated with C atoms in different sublattices in graphene, so that, in perfect agreement with Lieb's theorem [17], the total magnetic moment of a carbon flake (neutral charge state) is simply the difference in the number of atoms on the two sublattices. The analysis of the electronic structure of the substitutional defects shows that the magnetism comes from spin-polarized defect-induced states in the gap, which are spatially localized at the defects. Our results also indicate that the magnetic moment can be varied by electrically charging the system, i.e., by changing the number of electrons in the quantum dots associated with the defects, as demonstrated in the insets presented in Fig. 4.

To conclude, using DFT simulations we showed that the electron-irradiation-mediated substitution of B/N atoms in *h*-BN nanostructures with C atoms is governed not only by the response of the system to irradiation, but also the energetics of different defect configurations, which explains the puzzling experimental observations [12,13,16] of C doping of *h*-BN systems. As the substitution process can be controlled by electrically charging the system during irradiation, our results indicate that by using a focused electron beam and simultaneously charging the sample one can manufacture spatially localized hybrid structures which should exhibit intriguing electronic properties [34,35], and controllable magnetism. This technique, which is a combination of electron irradiation and beam-assisted deposition of the material deliberately introduced into the TEM chamber, can be applied to any 2D material (or 1D systems like nanotubes), including recently reported inorganic 2D structures [36].

We thank D. Golberg, K. Suenaga, S. Riikonen, and J. C. Meyer for useful discussions. This work was supported by the Academy of Finland through Centre of Excellence and other projects. The also acknowledge Finnish IT Center for Science for generous grants of computer time.

[1] A. K. Geim and K. S. Novoselov, Nature Mater. **6**, 183 (2007).
[2] A. H. Castro Neto *et al.*, Rev. Mod. Phys. **81**, 109 (2009).
[3] D. Pacilé *et al.*, Appl. Phys. Lett. **92**, 133107 (2008).
[4] N. Alem *et al.*, Phys. Rev. B **80**, 155425 (2009).
[5] K. Watanabe, T. Taniguchi, and H. Kanda, Nature Mater. **3**, 404 (2004).
[6] A. L. M. Reddy *et al.*, ACS Nano **4**, 6337 (2010).
[7] X. Wang *et al.*, Science **324**, 768 (2009).
[8] J. C. Meyer *et al.*, Nature Mater. **10**, 209 (2011).
[9] L. Ci *et al.*, Nature Mater. **9**, 430 (2010).
[10] M. Kawaguchi, T. Kawashima, and T. Nakajima, Chem. Mater. **8**, 1197 (1996).
[11] K. Yuge, Phys. Rev. B **79**, 144109 (2009).
[12] X. Wei, M. Wang, Y. Bando, and D. Golberg, J. Am. Chem. Soc. **132**, 13592 (2010).
[13] X. Wei, M. Wang, Y. Bando, and D. Golberg, ACS Nano **5**, 2916 (2011).
[14] A. Zobelli *et al.*, Phys. Rev. B **75**, 245402 (2007).
[15] J. Kotakoski *et al.*, Phys. Rev. B **82**, 113404 (2010).
[16] O. L. Krivanek *et al.*, Nature (London) **464**, 571 (2010).
[17] E. H. Lieb, Phys. Rev. Lett. **62**, 1201 (1989).
[18] G. Kresse and J. Furthmüller, Comput. Mater. Sci. **6**, 15 (1996).
[19] P. E. Blöchl, Phys. Rev. B **50**, 17 953 (1994).
[20] J. P. Perdew, K. Burke, and M. Ernzerhof, Phys. Rev. Lett. **77**, 3865 (1996).
[21] J. Heyd, G. E. Scuseria, and M. Ernzerhof, J. Chem. Phys. **118**, 8207 (2003).
[22] O. Cretu *et al.*, Phys. Rev. Lett. **105**, 196102 (2010).
[23] A. V. Krasheninnikov *et al.*, Phys. Rev. Lett. **102**, 126807 (2009).
[24] J. Lento *et al.*, J. Phys. Condens. Matter **14**, 2637 (2002).
[25] J. Shim *et al.*, Phys. Rev. B **71**, 245204 (2005).
[26] S. Lany and A. Zunger, Phys. Rev. B **78**, 235104 (2008).
[27] X. Blase *et al.*, Phys. Rev. B **51**, 6868 (1995).
[28] P. Piquini *et al.*, Nanotechnology **16**, 827 (2005).
[29] M. H. Evans, J. D. Joannopoulos, and S. T. Pantelides, Phys. Rev. B **72**, 045434 (2005).
[30] A. V. Krasheninnikov and F. Banhart, Nature Mater. **6**, 723 (2007).
[31] J. C. Meyer *et al.*, Nano Lett. **9**, 2683 (2009).
[32] C. Jin *et al.*, Phys. Rev. Lett. **102**, 195505 (2009).
[33] W. L. Wang, S. Meng, and E. Kaxiras, Nano Lett. **8**, 241 (2008).
[34] J. Li and V. B. Shenoy, Appl. Phys. Lett. **98**, 013105 (2011).
[35] J. M. Pruneda, Phys. Rev. B **81**, 161409 (2010).
[36] J. Coleman *et al.*, Science **331**, 568 (2011).